

20 transformations are equivalent to randomizing particle travel time or relative velocity for each
21 model time step. Here, the time randomizing procedure known as subordination is applied to
22 flow field output from MODFLOW simulations. Numerical tests check the applicability of the
23 novel method in mapping regional-scale super-diffusive transport conditioned on local properties
24 of multi-dimensional heterogeneous media.

25 **Key Words:** Super-diffusion, Subordination, Regional flow, Lagrangian solver

26 **1. Introduction**

27 Groundwater contamination is a world-wide problem that frequently involves regional-
28 scale transport processes. The groundwater flow and transport models used to simulate and
29 predict contaminant transport are, by definition, simplifications of reality and can only account
30 for aquifer heterogeneity down to a finite level. Thus, the homogeneous grid cells of regional
31 flow models can be much larger than the Darcy, or theoretical representative elementary volume,
32 scale. Thus, local dispersion in a regional-scale transport model is typically assumed to be
33 Fickian, unless additional treatment (such as the kernel used in the convolution of solute
34 concentration [*Neuman and Tartakovsky, 2009*]) is used.

35 If we had perfect knowledge of aquifer heterogeneity and could develop perfect
36 representations of this heterogeneity in numerical simulations, then an equation for particle
37 advection would be all that is required to simulate transport. The variability in particle transport
38 velocities would be driven by changes in hydraulic conductivity. An advection-dispersion
39 equation (ADE) model allows for analytical or numerical incorporation of particle spreading
40 around the advective velocities. There are bounds, however, on how extreme or skewed
41 dispersion can be under the Fickian (classical ADE) model. There have been different methods
42 proposed to address proper model treatment of various types of heterogeneity in groundwater,

43 including the upscaling approach [*Bellin et al.*, 2004; *Pruess*, 2004; *Zhang et al.*, 2010; *Zyvoloski*
44 *et al.*, 2008] and the statistics based, downscaling method [*Lu et al.*, 2003; *Lu et al.*, 2002;
45 *Ramanathan et al.*, 2008; *Ramanathan et al.*, 2010; *Sun et al.*, 2008]. Similar upscaling
46 approaches have also been used for other environmental transport areas such as surface
47 hydrology [*Barrios and Frances*, 2012; *Hansen et al.*, 2007] and atmospheric sciences [*Cassiani*
48 *et al.*, 2010; *Karamchandani et al.*, 2009].

49 This study focuses on a new and relatively simple way of incorporating fractional
50 advection-dispersion equation (fADE) models of transport into regional numerical models in
51 order to move application of anomalous transport theory beyond academic study into application.
52 The space fADE models are generalizations of classical ADE models that can parsimoniously
53 incorporate extreme variation in particle velocities by replacing explicit representation of
54 heterogeneity with a fractional derivative [*Meerschaert et al.*, 1999a]. It was previously observed
55 that, more generally, the fractional power of the advection-dispersion operator leads to super-
56 diffusion [*Baeumer et al.*, 2001] and its analytical solution could be obtained by transforming the
57 solution to the classical ADE model. This transformation, known as subordination, amounts to
58 randomizing the velocity of each particle for each time step. However in that model super-
59 diffusive spread is present in all directions. One way to obtain governing equations whose
60 solutions are super-diffusive in the direction of flow but diffuse normally in all other directions is
61 to treat the fractional power of the advection operator and the diffusion operator separately; for
62 the precise mathematical framework see [*Baeumer et al.*, 2009]. For a more general CTRW
63 formulation that is faithful to the local velocity field, see *de Anna et al.* [2013].

64 While previous work demonstrated the subordination technique for analytical models, we
65 adapt it here for use with numerical particle tracking techniques amenable to simulation of

66 transport subject to complex boundary and initial conditions. The goal is to apply subordination
67 techniques to the velocity field output from a MODFLOW [Harbaugh *et al.*, 2000] simulation
68 (or any other solutions of velocity using the finite difference method), thus incorporating sub-
69 grid heterogeneity into a particle tracking transport model. The method is coded into “Sub-
70 RWHet”, which is a Lagrangian solver combining Darcy-scale non-Fickian diffusion with
71 coarsely resolved velocity fields. This particle tracking code is especially useful for evaluating
72 time to breakthrough at a sensitive receptor in cases where the classical ADE (applied to a coarse
73 regional grid) underestimates the early arrivals of contaminants.

74 The subordination method has also been used to produce sub-diffusion [Baeumer and
75 Meerschaert, 2001; Schumer *et al.*, 2003; Sokolov and Metzler, 2004] by changing the form of
76 the transformation. In this case, subordination gives a wide distribution of travel times,
77 producing a retardation-like effect with power-law tailing of breakthrough curves and works
78 independently to the spatial dispersion operator used in the physical model. This article focuses
79 on super-diffusion along flow lines and leaves extensions that include retardation effects for a
80 future study.

81 **2. Methodology development: Subordination in the direction of flow**

82 **2.1. Previous physical models**

83 We first review briefly the limitations of previous models in capturing sub-grid anomalous
84 super-diffusion. In one dimension the spatial fractional derivative has been used to capture
85 super-diffusion due to fast motion of solutes along preferential flow paths [Benson *et al.*, 2000a;
86 Chaves, 1998]

$$87 \quad \frac{\partial}{\partial t} u(t, x) = -v \frac{\partial u(t, x)}{\partial x} + D \frac{\partial^\alpha u(t, x)}{\partial x^\alpha}, \quad (1)$$

88 with the initial condition $u(0,x)=u_0(x)$ and scale index $1 < \alpha \leq 2$. Here v is the mean flow
 89 velocity, D is the dispersion coefficient, and u denotes the solute concentration. When $\alpha = 2$,
 90 the above space fADE reduces to the classical 2nd-order ADE.

91 In the fractional calculus framework, a mixing measure (denoted as M) has been used to
 92 generalize this concept to higher dimensions by collating all the different fractional directional
 93 derivatives [Meerschaert *et al.*, 1999b]

$$94 \quad D_M^\alpha f(\mathbf{x}) = \int_{|\theta|=1} \frac{d^\alpha}{ds^\alpha} f(\mathbf{x} + s\theta) M(d\theta), \quad (2)$$

95 where different order derivatives in different directions are captured by a full operator-stable
 96 fractional derivative D_M^α [Meerschaert *et al.*, 2001]. The variable s in equation (2) denotes the
 97 parameter describing distance travelled into the θ direction. One major drawback to these models
 98 is that the direction θ is fixed in the integrand of the operator, and therefore $D_M^\alpha f$ is a mixture
 99 of values of f along *straight* lines to infinity irrespective of the conductivity field. While this
 100 method produces reasonable particle trajectories in a multidimensional fractured rock setting
 101 where the fracture orientation remains constant in space [Reeves *et al.*, 2008; Zhang *et al.*, 2010],
 102 in general this is not desirable. A spatially dependent spectral measure requires straight line
 103 jumps, which is not physically realistic, so it was also suggested that a streamline projection
 104 method be used. In this method, the local dispersion coefficient at a point x would determine the
 105 total dispersive jump size over a time period dt (irrespective of the local speed downstream as the
 106 jump size distribution is based on the dispersion coefficient at the initial particle position) while
 107 the jump direction varies with the flow field [Zhang *et al.*, 2006].

108 2.2. Development of the new physical model

109 We propose to model the influence of sub-grid heterogeneity not through randomizing
110 jump distances but through randomizing *individual relative velocities*; i.e., having faster and
111 slower particles. In other words, if we assume a particle following the flow at a given velocity is
112 at position $X(t)$ by time t , an s -times faster particle would be already at position $X(st)$. The
113 proportion of fast and slow particles is given according to the one-dimensional stochastic process
114 that best models sub-grid heterogeneity in case of uniform flow. We call $\tau = st$ the *operational*
115 *time* and the density of the one-dimensional stochastic process the *subordinator* and the resulting
116 two or three dimensional process the *subordinated flow*.

117 It is important to note that when fast pathways are present, sub-grid heterogeneity might
118 have a much bigger impact in the direction of flow than in other directions, while trapping of
119 particles hinders movement of particles to any direction. Therefore we separate the random
120 dispersive displacement (by subordination regional flow) from molecular (lateral) diffusion. The
121 hydrodynamic dispersion contains mechanical dispersion and molecular diffusion. A larger local
122 flux is more likely to transport the solute particle further downstream along the streamline. In
123 other words, the super-diffusive jumps are not just related to the magnitude and direction of local
124 flux but to the properties of the material that particles have to jump through.

125 We assume that the subordinating process is infinitely divisible, i.e., transport during
126 uniform flow conditions on a grid level consists of many independent identically distributed
127 random jumps. This implies that the Fourier transform of the subordinator g satisfies

$$128 \quad \frac{\partial}{\partial t} \hat{g}(t, k) = \psi(ik) \hat{g}(t, k); \hat{g}(t, k) = 1 \quad (3)$$

129 where ψ is the log-characteristic function of the subordinating process. For example, for
 130 classical normalized advection (normalized to have velocity one, implying operational time is
 131 equal to regular time), $\psi_1(ik) = -ik$, for classical normalized advection and dispersion,
 132 $\psi_2(ik) = -ik + D(ik)^2$, for normalized advection and fractional dispersion,
 133 $\psi_\alpha(ik) = -ik + D(ik)^\alpha$, $1 < \alpha \leq 2$ [Benson et al., 2000b], and for normalized advection and
 134 tempered fractional dispersion $\psi_{\alpha,\lambda}(ik) = -(1 + \alpha D \lambda^{\alpha-1})ik + D(ik + \lambda)^\alpha - D\lambda^\alpha$, $1 < \alpha \leq 2$
 135 [Baeumer and Meerschaert, 2010; Cartea and del-Castillo-Negrete, 2007; Koponen, 1995]. For
 136 the case of fractional advection $\psi(ik) = -(ik)^\alpha$, $0 < \alpha \leq 1$, subordinating in any direction was
 137 already investigated in Baeumer et al.[2001]. Note that except for the first and last case, the
 138 support of g is the whole real line which means that negative operational times have to be
 139 admissible. As only flow without dispersion is time reversible (going upstream), this restricts the
 140 applicability of these subordinators to the flow direction.

141 If transport in the flow field is given by
 142 $\frac{\partial}{\partial t} u(t, \mathbf{x}) = -\nabla \cdot (\mathbf{v}(\mathbf{x})u(t, \mathbf{x})) = -\nabla_{\mathbf{v}(\mathbf{x})} u(t, \mathbf{x}); u(0, \mathbf{x}) = u_0(\mathbf{x})$, then the subordinated flow is
 143 governed by

$$144 \quad \frac{\partial}{\partial t} u(t, \mathbf{x}) = \psi(\nabla_{\mathbf{v}(\mathbf{x})}) u(t, \mathbf{x}); u(0, \mathbf{x}) = u_0(\mathbf{x}), \quad (4)$$

145 where $\psi(\nabla_{\mathbf{v}(\mathbf{x})})$ is a differential operator defined through a functional calculus [Baeumer et al.,
 146 2009]. For example, if ψ_2 is as above,

$$147 \quad \psi_2(\nabla_{\mathbf{v}}) = -\nabla_{\mathbf{v}} + D(\nabla_{\mathbf{v}})^2.$$

148 By definition, the solution to (4) is given by subordination; i.e. if u_1 is the solution to

149
$$\frac{\partial}{\partial t} u_1(t, \mathbf{x}) = -\nabla_{\mathbf{v}(\mathbf{x})} u_1(t, \mathbf{x}); u_1(0, \mathbf{x}) = u_0(\mathbf{x}) \quad (5)$$

150 and g_ψ is the subordinator; i.e. g_ψ solves (3), then

151
$$u_\psi(t, \mathbf{x}) = \int g_\psi(t, \tau) u_1(\tau, \mathbf{x}) d\tau \quad (6)$$

152 solves (4).

153 Now that we know how to handle subordination in the flow direction, we can add lateral
154 diffusion to the governing equation and try to solve

155
$$\frac{\partial}{\partial t} u(t, \mathbf{x}) = \psi \left(\nabla_{\mathbf{v}(\mathbf{x})} \right) u(t, \mathbf{x}) + \nabla \cdot D \nabla u(t, \mathbf{x}); u(0, \mathbf{x}) = u_0(\mathbf{x}). \quad (7)$$

156 Model (7) is the new physical model proposed by this study. In the following we approximate
157 and apply it.

158 The Markovian model governed by (7) can now be further extended to include particle
159 trapping, mobile/immobile extensions, reaction terms, etc., by using, for example, fractional
160 temporal derivatives. This is straight forward as the operator on the right hand side of (7) is still a
161 tractable linear generator of an analytic, dissipative semigroup. Since this study focuses on
162 super-diffusion, we leave properties of these extensions of (7) to a future study.

163

164 **2.3. Numerical approximations**

165 The solution of model (7) can be approximated using the operator splitting method. First,
166 approximate by time stepping, advancing in each time step according to (7) with $D=0$ and $u_0(\mathbf{x})$
167 being the current state, and then according to (7) with $\psi = 0$ [Baeumer *et al.*, 2009]. For faster

168 convergence, the order can be alternated [Strang, 1968]. Instead of subordinating to obtain the
 169 solution to (7) with $D=0$ at a small time step, one can use a numerical approximation of
 170 $\psi(\nabla_{\mathbf{v}(\mathbf{x})})$ and approximate (implicitly) via $u_\psi(dt, \mathbf{x}) = u_0(\mathbf{x}) + dt\psi(\nabla_{\mathbf{v}(\mathbf{x})})u_\psi(dt, \mathbf{x})$. Numerical
 171 approximations of $\psi(\nabla_{\mathbf{v}(\mathbf{x})})$ can be obtained by transferring shift invariant numerical
 172 approximations of $\psi\left(\frac{d}{dx}\right)$ onto flow lines; i.e. if $\psi\left(\frac{d}{dx}\right)f(x) = \lim_{h \rightarrow 0} \sum_j w_{h,j} f(x - y_{h,j})$ for
 173 some weights $w_{h,j}$ and shifts $y_{h,j}$, then

$$174 \quad \psi(\nabla_{\mathbf{v}(\mathbf{x})})(f)(\mathbf{x}) = \lim_{h \rightarrow 0} \sum_j w_{h,j} u_1(y_{h,j}, \mathbf{x}) \quad (8)$$

175 [Baeumer et al., 2009]. The solution can also be approximated by using a particle tracking code
 176 such as the one described below, alternatively jumping along the flow line for a time period dt
 177 with relative particle speed given by the subordinator, and jumping for a time period dt according
 178 to the multivariate Brownian motion with generator $\nabla \cdot D \nabla$.

179 3. Particle tracking approach

180 We propose a 4-step Lagrangian scheme to subordinate regional-scale flow, after
 181 MODFLOW is used to solve the steady-state or transient flow field. We subordinate according to
 182 the most general model mentioned in Section 2, the tempered stable model:

$$183 \quad \psi(ik) = \psi_{\alpha, \lambda}(ik) = -(1 + \alpha D \lambda^{\alpha-1})ik + D(ik + \lambda)^\alpha - D\lambda^\alpha, 1 < \alpha \leq 2.$$

184 The following particle-tracking algorithms are coded into RWHet [LaBolle, 2006], which is a
 185 mature Random Walk solver for simulating solute transport in heterogeneous porous media that
 186 has undergone significant model validation [Zhang et al., 2012]:

187 1) Calculate the operational time for each particle during the k -th jump:

$$188 \quad \delta t_k = dt_k + (\sigma_R dt_k)^{1/\alpha} dL_{\alpha,\lambda} (\beta = +1, \sigma = 1, \mu = 0) \quad (9)$$

189 where $dt_k [T]$ denotes the user-defined time step (which is adjusted further in RWHet to account
 190 for the boundary condition and transient flow, etc.), $\sigma_R [T^{\alpha-1}]$ is a measure of uncertainty and
 191 $dL_{\alpha,\lambda}$ [dimensionless] is an α -stable tempered random variable with skewness $\beta = +1$, scale
 192 $\sigma = 1$, shift $\mu = 0$, and truncation parameter λ (see *Baeumer and Meerschaert [2010]* on
 193 generation techniques).

194 2) Track the advective displacement of the particle along the present stream lines for the
 195 operational time $\delta t_k [T]$. Note that we may need to divide δt_k into sub-time steps (depending
 196 on the magnitude of local velocities) to remain on the flow line, and relocate the particle around
 197 the grid interface. In addition, the operational time δt_k can be either positive or negative, since
 198 the scale index α is large than 1. Hence we reverse the flow field and track the backward
 199 motion of the particle when $\delta t_k < 0$.

200 3) Calculate the lateral dispersion (i.e., the concentration-gradient driven diffusion) for
 201 each particle during the time step dt_k using the Itô-Euler integration scheme [*Gardiner, 1985*]:

$$202 \quad dX_i = \left[\frac{\partial}{\partial x_i} D_{ij}(X, t) \right] dt_k + B_{ij}(X, t) d\omega_j(dt_k) \quad (10)$$

203 where $i, j = 1, 2, 3$ denotes the three axes in space, $\omega_j [T^{1/2}]$ (a Wiener process) is a vector of
 204 independent normally-distributed random variables with zero mean and variance
 205 $\langle d\omega_i, d\omega_j \rangle = \delta_{ij} dt_k$, $B_{ij} [LT^{1/2}]$ is a tensor defining the strength of diffusion ($2D_{ij} = B_{ik} B_{kj}$).

206 Here we assume that the medium porosity is constant. This step has already been coded into
 207 RWHet [LaBolle, 2006] by its author.

208 4) Update particle and grid properties, and iterate steps 1-3 until reaching the end of
 209 simulation, or until all particles exit the model domain.

210 4. Numerical experiments: Validation and application

211 We validated extensively the methods described above. Two numerical experiments are
 212 shown below.

213 4.1. Example 1

214 This example non-trivially tests the 1- d concentration profile (snapshot) simulated by Sub-
 215 RWHet along a straight streamline with local average velocity, which is two orders of magnitude
 216 lower around $x=-1/2$ and $x=3/2$ than at other locations due to, for example, a change in porosity
 217 (see Figure 1a). The transport model (7) along the x -axis is now reduced to

$$218 \quad \frac{\partial}{\partial t} u(t, x) = -V(x) \frac{\partial}{\partial x} u(t, x) + \sigma_R \left[V(x) \frac{\partial}{\partial x} \right]^\alpha u(t, x), \quad (11)$$

219 where we take $\sigma_R = 0.1$ for this example, and the lateral diffusion coefficient $D=0$ is ignored to
 220 focus on the subordinated flow. The analytical solution on the infinite domain is given by

$$221 \quad u(t, x) = \frac{1}{(\sigma t)^{1/\alpha}} g_\alpha \left(\frac{T_x - t}{(\sigma t)^{1/\alpha}} \right); T_x = \int_{x_0}^x \frac{1}{V(\xi)} d\xi$$

222 where g_α is the standard skewed α -stable density with Fourier transform $\hat{g}(k) = e^{(ik)^\alpha}$. The
 223 analytical solution can be accurately approximated using standard codes for computing α -stable
 224 densities.

225 The numerical model consists of 400 columns, 1 row, and 1 layer. The cell width along
226 rows is $\Delta x=0.01$, the cell width along column is $\Delta y=1$, and the layer thickness is $\Delta z =1$. An
227 instantaneous point source (with 10^6 particles) at time $t=0$ is located at position $x_0 = -1.5$. The
228 1- d model domain is $[-2, 2]$. For the transport model, the left boundary (as $x = -2$) is treated as a
229 reflective boundary, where the particle exiting the left boundary (due to backward transport,
230 since the flow is from left to right) is reflected back to the model domain. The right boundary is
231 an absorbing boundary. To account for the change in porosity the particle count needs to be
232 normalized by dividing it by the porosity. In a 2- d divergence free (constant porosity) field this
233 would automatically be achieved by a varying flow line density. Numerical solutions of Sub-
234 RWHet generally match the analytical solutions (Fig. 1b,c). The noise in the simulated snapshot
235 with low concentrations can be improved by either increasing the number of particles, or using
236 the particle splitting technique. Note not only the presence of downstream concentration, where
237 there is none in the $\alpha=2$ case, but also the drop-off in concentration after the slow zones
238 highlighting that slow zones affect the fractional dispersion; i.e. even particles with high relative
239 velocities are going slowly.

240

241 **4.2. Example 2**

242 Example 2 considers flow and transport in a 2- d heterogeneous aquifer, to test the
243 applicability of Sub-RWHet to solve complicated problems where either the analytical solutions
244 or other numerical solvers are not available. The flow model configuration is shown in Fig. 2a,
245 where ground water flows from top to bottom (bounded by the two vertical no-flow boundaries).
246 Water is injected (at a rate $Q=0.09 \text{ m}^3/\text{s}$) into the aquifer through a fully penetrating well near the
247 top boundary, and an extraction well (at a pumping rate $Q=1.16 \text{ m}^3/\text{s}$) is located near the bottom

248 boundary. The two wells are separated by a low-permeability zone whose hydraulic conductivity
249 is 3-orders of magnitude smaller than the surrounding high-permeability material. A similar
250 model setup was used by *Zheng and Wang* [1999].

251 We first check whether the subordinated particle trajectories follow streamlines. Results
252 show that Sub-RWHet captures precisely the position of random-walking particles along
253 streamlines at various times (Fig. 2b~d). The model solved for this case is equation (7) without
254 the lateral dispersion term (the last term on the right-hand side of (7)). The calculated advective
255 displacement of each particle generally follows the streamlines, which diverge or converge due
256 to the injection and pumping of groundwater.

257 We then check whether Sub-RWHet can capture the super-diffusive transport. A
258 continuous source with unit concentration is injected at the injection well. Both RWHet and
259 Sub-RWHet are used to track contaminant particles through the heterogeneous medium. The
260 water injection rate for this case is changed to $0.001 \text{ m}^3/\text{s}$, and the extraction rate at the pumping
261 well is $0.0189 \text{ m}^3/\text{s}$ (as in *Zheng and Wang* [1999]). The simulated particle plumes are shown in
262 Fig. 3, where the subordinated plume has a relatively faster leading edge, as expected.

263 **5. Conclusions**

264 In cases where ADE-based numerical models overestimate solute travel times for the
265 leading edge of a plume, alternative models that can simulate super-diffusion are needed for
266 more accurate risk characterization. This study derives a novel physical model (eq. (7)) which
267 combines local and nonlocal transport by subordinating regional flow. The sub-grid dispersion is
268 not limited to the Fickian case, but can rather be a wide range of dispersive processes varying
269 from super-diffusion to normal diffusion. Numerical approximations using both the operator-
270 split time-stepping method and the particle tracking method are provided, where numerical

271 experiments of the latter are shown for demonstration. The resultant Lagrangian solver “Sub-
272 RWHet” accounts for the sub-grid super-diffusion, and it can read grid-based velocity fields
273 generated for example by the popular USGS code MODFLOW. An executable Sub-RWHet is
274 available upon request from the authors.

275 It is noteworthy that the new physical model (7) and its solver extend the previous
276 approach for modeling space-dependent anomalous super-diffusion [Zhang *et al.*, 2006]. The
277 dispersion coefficient in model (7) is not limited to a constant, but can vary in space and/or time.
278 To the best of our knowledge, it is therefore the first Lagrangian model that allows multi-
279 dimensional super-diffusion conditioned on local aquifer properties. On the other hand, model
280 (7) and the other fractional-derivative models are now limited to fitting models, where the
281 quantitative linkage between medium heterogeneity and model parameters remains to be shown.
282 We will focus on the model predictability in a future study.

283 **Acknowledgement:** We would like to thank Dr M. Kovács for many helpful discussions.
284 YZ was supported by the Desert Research Institute and the National Science Foundation under
285 Grant DMS-1025417. YZ thanks Dr. E. M. LaBolle for providing his code RWHet. The
286 copyright of the original RWHet belongs to LaBolle. This paper does not necessarily reflect the
287 views of the funding organizations.

288 **References**

- 289 Baeumer, B., and M. M. Meerschaert (2001), Stochastic solutions for fractional Cauchy
290 problems, *Fractional Calculus and Applied Analysis*, 4(4), 481-500.
291 Baeumer, B., and M. M. Meerschaert (2010), Tempered stable Levy motion and transient super-
292 diffusion, *Journal of Computational and Applied Mathematics*, 233(10), 2438-2448, doi:
293 10.1016/j.cam.2009.10.027.
294 Baeumer, B., M. Haase, and M. Kovacs (2009), Unbounded functional calculus for bounded
295 groups with applications, *Journal of Evolution Equations*, 9(1), 171-195, doi:
296 10.1007/s00028-009-0012-z.

297 Baeumer, B., M. M. Meerschaert, D. A. Benson, and S. W. Wheatcraft (2001), Subordinated
298 advection-dispersion equation for contaminant transport, *Water Resources Reserach*,
299 37(6), 1543-1550.

300 Barrios, M., and F. Frances (2012), Spatial scale effect on the upper soil effective parameters of
301 a distributed hydrological model, *Hydrological Processes*, 26(7), 1022-1033, doi:
302 10.1002/hyp.8193.

303 Bellin, A., A. E. Lawrence, and Y. Rubin (2004), Models of sub-grid variability in numerical
304 simulations of solute transport in heterogeneous porous formations: three-dimensional
305 flow and effect of pore-scale dispersion, *Stochastic Environmental Research and Risk
306 Assessment*, 18(1), 31-38, doi: 10.1007/s00477-003-0164-2.

307 Benson, D. A., S. W. Wheatcraft, and M. M. Meerschaert (2000a), Application of a fractional
308 advection-dispersion equation, *Water Resources Reserach*, 36(6), 1403-1412.

309 Benson, D. A., S. W. Wheatcraft, and M. M. Meerschaert (2000b), The fractional-order
310 governing equation of Lévy motion, *Water Resources Reserach*, 36(6), 1413-1423.

311 Cartea, A., and D. del-Castillo-Negrete (2007), Fluid limit of the continuous-time random walk
312 with general Levy jump distribution functions, *Physical Review E*, 76(4), doi:
313 10.1103/PhysRevE.76.041105.

314 Cassiani, M., J. F. Vinuesa, S. Galmarini, and B. Denby (2010), Stochastic fields method for
315 sub-grid scale emission heterogeneity in mesoscale atmospheric dispersion models,
316 *Atmospheric Chemistry and Physics*, 10(1), 267-277.

317 Chaves, A. S. (1998), A fractional diffusion equation to describe Lévy flights, *Physical Letters
318 A*, 239, 13-16.

319 de Anna, P., T. Le Borgne, M. Dentz, A. M. Tartakovsky, D. Bolster, and P. Davy (2013), Flow
320 Intermittency, Dispersion, and Correlated Continuous Time Random Walks in Porous
321 Media, *Physical Review Letters*, 110(18), 184502, doi:10.1103/PhysRevLett.110.184502.

322 Gardiner, C. W. (1985), *Handbook of Stochastic Processes for Physics, Chemistry, and the
323 Natural Sciences*, 2nd ed., Springer-Verlag, New York.

324 Hansen, J. R., J. C. Refsgaard, S. Hansen, and V. Ernstsen (2007), Problems with heterogeneity
325 in physically based agricultural catchment models, *Journal of Hydrology*, 342(1-2), 1-16,
326 doi: 10.1016/j.jhydrol.2007.04.0161.

327 Harbaugh, A. W., E. R. Banta, M. C. Hill, and M. G. McDonald (2000), MODFLOW-2000, The
328 U.S. Geological Survey Modular Ground-Water Model-- User guide to modularization
329 concepts and the ground-water flow processs *U.S. Geological Survey Open-File Report
330 00-92*, Reston, VA.

331 Karamchandani, P., K. Lohman, and C. Seigneur (2009), Using a sub-grid scale modeling
332 approach to simulate the transport and fate of toxic air pollutants, *Environmental Fluid
333 Mechanics*, 9(1), 59-71, doi: 10.1007/s10652-008-9097-0.

334 Koponen, I. (1995), Analytic approach to the problem of convergence of truncated Levy flights
335 towards the Gaussian stochastic-process, *Physical Review E*, 52(1), 1197-1199, doi:
336 10.1103/PhysRevE.52.1197.

337 LaBolle, E. M. (2006), RWHet: Random Walk Particle Model for Simulating Transport in
338 Heterogeneous Permeable Media, Version 3.2 User's Manual and Program
339 Documentation. Davis, CA.

340 Lu, S. L., F. J. Molz, and H. H. Liu (2003), An efficient, three-dimensional, anisotropic,
341 fractional Brownian motion and truncated fractional Levy motion simulation algorithm

342 based on successive random additions, *Computers & Geosciences*, 29(1), 15-25, doi:
 343 10.1016/s0098-3004(02)00073-0.
 344 Lu, S. L., F. J. Molz, G. E. Fogg, and J. W. Castle (2002), Combining stochastic facies and
 345 fractal models for representing natural heterogeneity, *Hydrogeology Journal*, 10(4), 475-
 346 482, doi: 10.1007/s10040-002-0212-x.
 347 Meerschaert, M. M., D. A. Benson, and B. Baeumer (1999a), Multidimensional advection and
 348 fractional dispersion, *Physical Review E*, 59(5), 5026-5028.
 349 Meerschaert, M. M., D. A. Benson, and B. Baumer (1999b), Multidimensional advection and
 350 fractional dispersion, *Physical Review E*, 59(5), 5026-5028, doi:
 351 10.1103/PhysRevE.59.5026.
 352 Meerschaert, M. M., D. A. Benson, and B. Baeumer (2001), Operator Lévy motion and
 353 multiscaling anomalous diffusion., *Physical Review E*, 63, 021112-021117.
 354 Neuman, S. P., and D. M. Tartakovsky (2009), Perspective on theories of non-Fickian transport
 355 in heterogeneous media, *Advances in Water Resources*, 32(5), 670-680, doi:
 356 10.1016/j.advwatres.2008.08.005.
 357 Pruess, K. (2004), A composite medium approximation for unsaturated flow in layered
 358 sediments, *Journal of Contaminant Hydrology*, 70(3-4), 225-247, doi:
 359 10.1016/j.jconhyd.2003.09.007.
 360 Ramanathan, R., R. W. Ritzi, Jr., and C. Huang (2008), Linking hierarchical stratal architecture
 361 to plume spreading in a Lagrangian-based transport model, *Water Resources Research*,
 362 44(4), doi: W0450310.1029/2007wr006282.
 363 Ramanathan, R., R. W. Ritzi, Jr., and R. M. Allen-King (2010), Linking hierarchical stratal
 364 architecture to plume spreading in a Lagrangian-based transport model: 2. Evaluation
 365 using new data from the Borden site, *Water Resources Research*, 46, doi:
 366 W0151010.1029/2009wr007810.
 367 Reeves, D. M., D. A. Benson, M. M. Meerschaert, and H.-P. Scheffler (2008), Transport of
 368 conservative solutes in simulated fracture networks: 2. Ensemble solute transport and the
 369 correspondence to operator-stable limit distributions, *Water Resources Research*, 44(5),
 370 doi: 10.1029/2008wr006858.
 371 Schumer, R., D. A. Benson, M. M. Meerschaert, and B. Baeumer (2003), Fractal
 372 mobile/immobile solute transport, *Water Resources Research*, 39(10), 1296-1308.
 373 Sokolov, I. M., and R. Metzler (2004), Non-uniqueness of the first passage time density of Levy
 374 random processes, *Journal of Physics A-Mathematical and General*, 37(46), L609-L615,
 375 doi: 10.1088/0305-4470/37/46/102.
 376 Strang, G. (1968), On the construction and comparison of difference schemes, *SIAM Journal on*
 377 *Numerical Analysis*, 5(3), 506--517.
 378 Sun, A. Y., R. W. Ritzi, and D. W. Sims (2008), Characterization and modeling of spatial
 379 variability in a complex alluvial aquifer: Implications on solute transport, *Water*
 380 *Resources Research*, 44(4), doi: 10.1029/2007wr006119.
 381 Zhang, Y., C. W. Gable, and B. Sheets (2010), Equivalent hydraulic conductivity of three-
 382 dimensional heterogeneous porous media: An upscaling study based on an experimental
 383 stratigraphy, *Journal of Hydrology*, 388(3-4), 304-320, doi:
 384 10.1016/j.hydrol.2010.05.009.
 385 Zhang, Y., E. M. LaBolle, D. M. Reeves, and C. Russell (2012), Development of RWHet to
 386 Simulate Contaminant Transport in Fractured Porous Media, 61 pp, DOE/NV/0000939-
 387 01, Report #45244.

388 Zhang, Y., D. A. Benson, M. M. Meerschaert, E. M. LaBolle, and H.-P. Scheffler (2006),
389 Random walk approximation of fractional-order multiscaling anomalous diffusion,
390 *Physical Review E*, 74(2), doi: 10.1103/PhysRevE.74.026706.

391 Zheng, C. M., and M. P. Wang (1999), MT3DMS: A Modular Three-Dimensional Multispecies
392 Transport Model, Documentation and User's Guide.

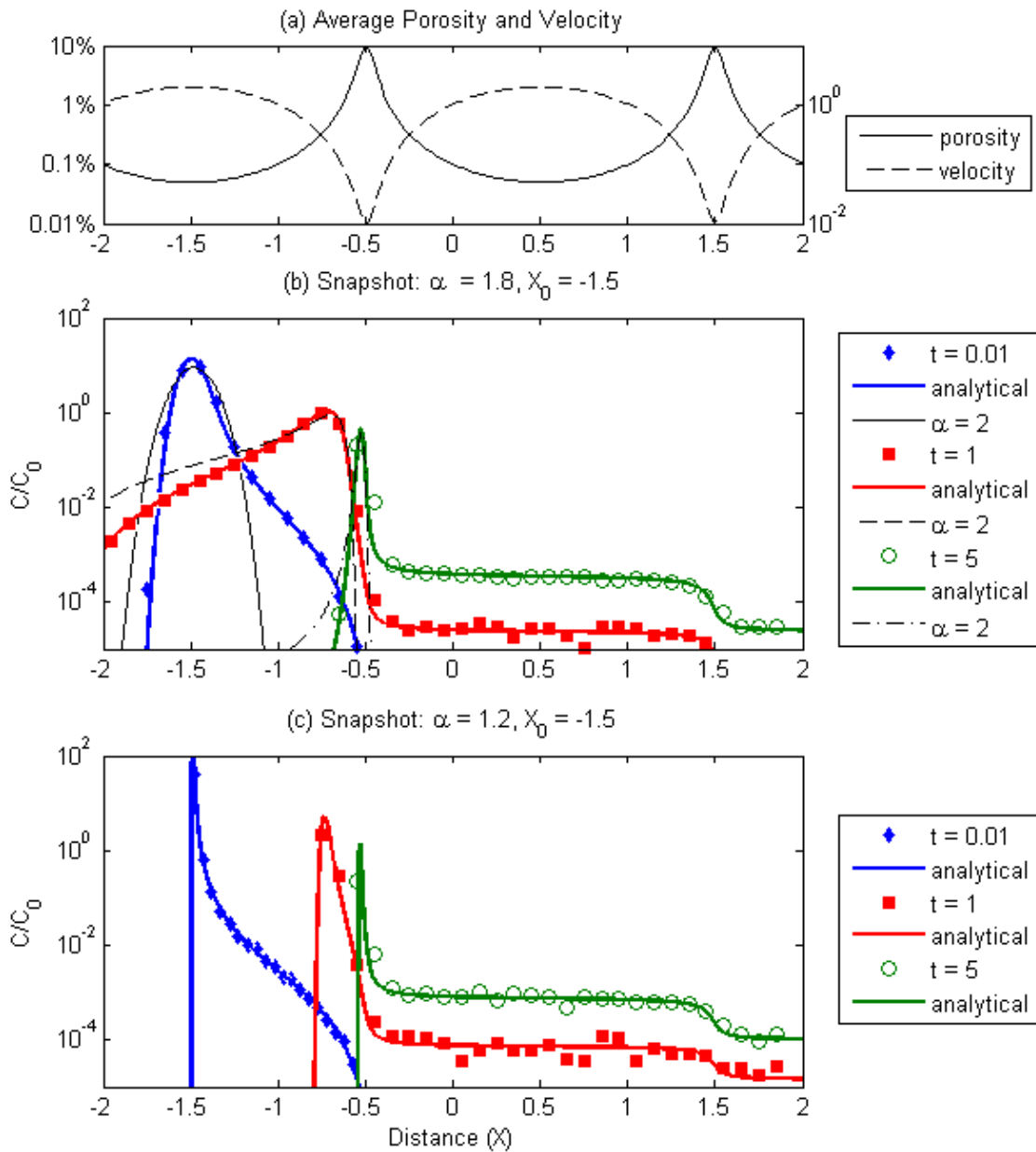
393 Zyvoloski, G. A., B. A. Robinson, and H. S. Viswanathan (2008), Generalized dual porosity: A
394 numerical method for representing spatially variable sub-grid scale processes, *Advances*
395 *in Water Resources*, 31(3), 535-544, doi: 10.1016/j.advwatres.2007.11.006.

396

397

398

Figure 1



400

401

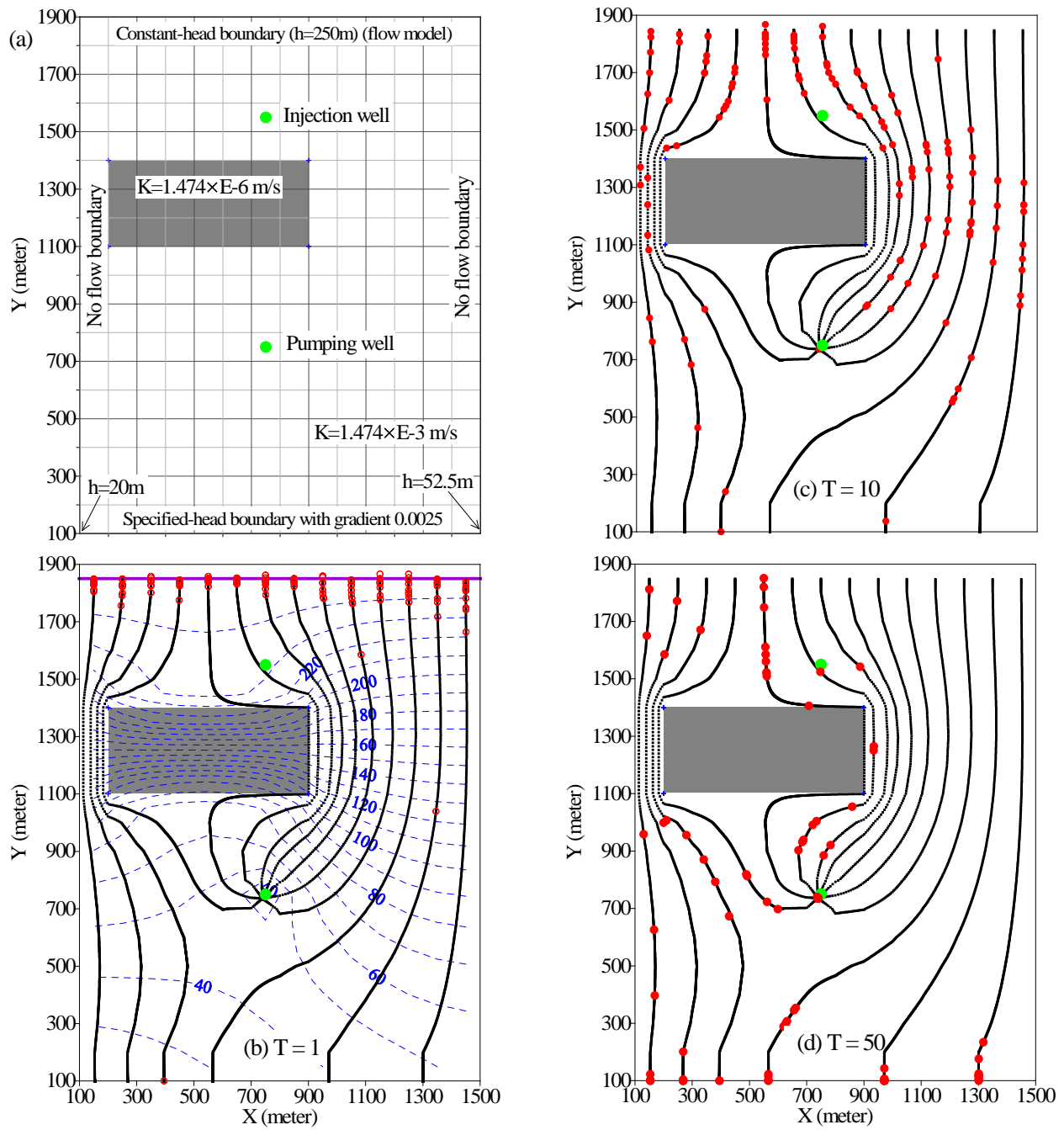
402

403

404

405

Figure 1. Example 1: Numerical solutions of Sub-RWHet (11) versus the analytical solution obtained by subordinating the solution to the advection equation for 1-d tracer snapshots for $\alpha=1.8$ (b) and $\alpha=1.2$ (c), respectively, for various times ($t=0.01, 1, \text{ and } 5$) injected at $x= -1.5$. Notice the heavy-tailed down-stream concentration being influenced by local low velocity zones. (a) shows the porosity and velocity.



407

408 Figure 2. Example 2: Numerical tests of Sub-RWHet: position of particles (red dots) at time T=1

409 day (b), 10 days (c), and 50 days (d). (a) shows the 2-d flow model. In (b), the dashed lines

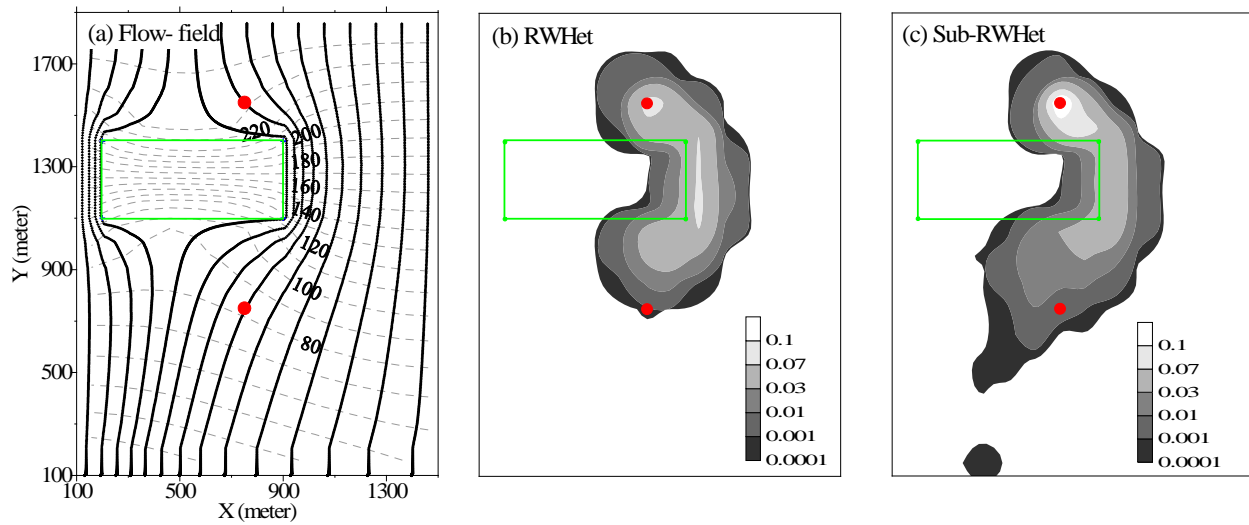
410 denote the simulated hydraulic head using MODFLOW. The solid lines in (b), (c) and (d)

411 are the streamlines calculated by RWHet. The green dots denote the location of two wells.

412

413

Figure 3



414

415

416 Figure 3. Example 2: The simulated particle plume (normalized concentration) at time T=10

417 days using RWHet (b) and Sub-RWHet (c), respectively, in a 2-d flow field (a).

418